Electronic Supplementary Material (ESI) for Journal of Materials Chemistry A.

Supporting Information

3D hierarchical core-shell spiny globe shaped Co_2P@Ni_2P/$NiCo_2O_4$@CoO for asymmetric supercapacitors

Wen-Wei Song,[a] Bing Wang,[a] Chen-Ning Li,[a] Shi-Ming Wang,[*b] and Zheng-Bo Han[*a]

[a] *College of Chemistry, Liaoning University, Shenyang 110036, P. R. China E-mail:*

ceshzb@lnu.edu.cn

[b] *Light Industry College, Liaoning University, Shenyang 110036, P. R. China E-mail：*

wangsm@lnu.edu.cn

Summary

1. Experimental

1.1. Synthesis

Synthesis of core-shell spiny globe with dodecahedron-shaped CC-NF

The ZC-NF can be converted into Co_3O_4/CoO-NF by a heat treatment at 350^oC for 2 h with a heating rate of 5^oC min^{-1} in an air atmosphere. The Co_3O_4/CoO-NF was denoted as CC-NF, and the XRD pattern of CC-NF is shown in Figure S9.

Synthesis of core-shell spiny globe with dodecahedron-shaped CCC-NF

The $NaH_2PO_2·H_2O$ (0.030 g, upstream side) and CC-NF (downstream) were placed in one porcelain boat and underwent a thermal treatment at 300^oC for 2 h with a heating rate of 2 ^oC min^{-1} in an Ar atmosphere to obtain Co_2P@Co_3O_4/CoO-NF (denoted as CCC-NF), and the XRD pattern of CCC-NF is shown in Figure S10.

Synthesis of core-shell spiny globe-shaped P-CNC-NF

The ZC-NF was soaked in the $Ni(NO_3)_2·6H_2O$ and $NaH_2PO_2·H_2O$ aqueous solution (2.8 g/L) for 24 h at room temperature to obtain Co_2P@Ni_2P@CoO-NF (denoted as P-CNC-NF), and the XRD pattern of P-CNC-NF is shown in Figure S11.

1.2. Calculations

Density function theory computational methods

The Vienna Ab Initio Package (VASP)[1,2] was employed to perform all the density functional theory (DFT) calculations within the generalized gradient approximation (GGA) using the PBE[3] formulation. The projected augmented wave (PAW) potentials[4, 5] were chosen to describe the ionic cores and take valence electrons into account using a plane wave basis set with a kinetic energy cutoff of 450 eV. Partial occupancies of the Kohn-Sham orbitals

were allowed using the Gaussian smearing method and a width of 0.05 eV. The electronic energy was considered self-consistent when the energy change was smaller than 10^{-4} eV. A geometry optimization was considered convergent when the force change was smaller than 0.05 eV/Å. Grimme's DFT-D3 methodology[6] was used to describe the dispersion interactions. During structural optimizations, the 2×2×1 Monkhorst-Pack k-point grid for Brillouin zone was used for k-point sampling for systems.

Calculations of single electrode

In a three-electrode system, the areal capacitance of electrode materials was calculated by following equation (1):

$$C_S = \frac{I\Delta t}{S\Delta V} \tag{1}$$

Where C_s (F cm^{-2}) is areal capacitance of electrode materials, Δt (s) represents discharge of galvanostatic charge-discharge, I (A) is discharge current, ΔV (V) is potential window during discharge process and S (cm^2) denotes load area of active materials.

In addition，the specific capacitance of electrode materials is calculated in a three-electrode system by following equation (2):

$$C_m = \frac{I\Delta t}{m\Delta V} \tag{2}$$

Where C_m (F g^{-1}) is specific capacitance of electrode materials and m (g) denotes the mass of active materials.

Calculations of ASCs device

In order to obtain better electrochemical performance of the device, according to charge balance following the relationship $Q_+ = Q_-$ of positive electron and negative electron, the mass rate of electron was calculated by following equations (3)-(5):

$$Q = C_m \times \Delta V \times m \tag{3}$$

$$Q_+ = Q_- \quad (4)$$

$$\frac{m^-}{m^+} = \frac{C^+ \times \Delta V^+}{C^- \times \Delta V^-} \quad (5)$$

Where Q is capacity, C_m represents specific capacitance of electrode materials, m (g) is the mass of active materials. C^+ and ΔV^+ denote specific capacitance and potential window of positive electrode. At the same time, C^- and ΔV^- denote specific capacitance and potential window of negative electrode.

$$E_m = \frac{1000 \times C_m \times \Delta V^2}{2 \times 3600} \quad (6)$$

$$P_m = \frac{3600 \times E_m}{\Delta t} \quad (7)$$

Where E_m (Wh kg^{-1}) is energy density, P_m (W kg^{-1}) is power density, ΔV (V) denotes potential window during the discharge process, C_m (F g^{-1}) represents specific capacitance of electrode materials and Δt (s) is discharge time of galvanostatic charge-discharge.

2. Supplementary Figures and Tables

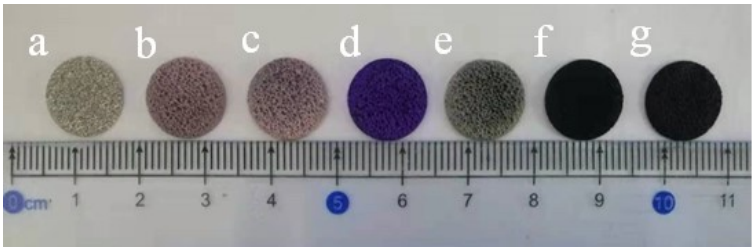

Figure S1. Images of a) NF, b) CF-NF, c) C-NF, d) ZC-NF, e) CNC-NF, f) NCC-NF, and g) CNNCC-NF.

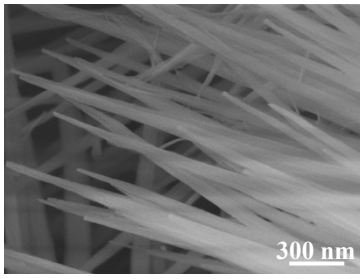

Figure S2. SEM image of C-NF.

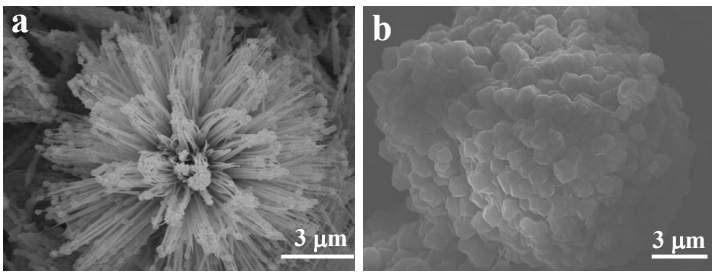

Figure S3. SEM images of a) ZIF-67/CoO-NF-1 (10 h), and b) ZIF-67/CoO-NF-3 (30 h).

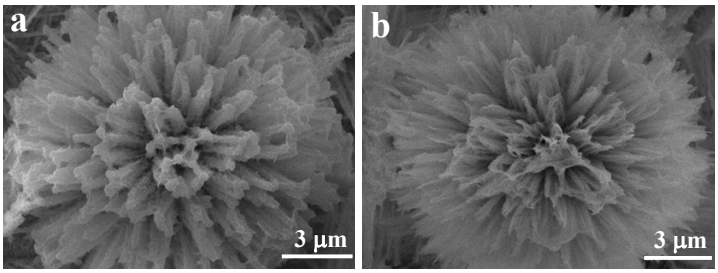

Figure S4. SEM images of a) Co-Ni LDH/CoO-NF-1 (12 h), and b) Co-Ni LDH/CoO-NF-3 (36 h).

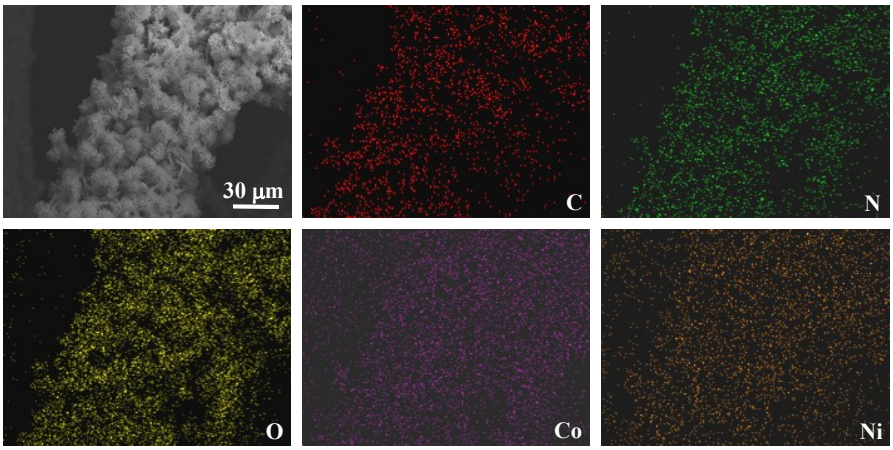

Figure S5. EDS elemental mapping of CNC-NF.

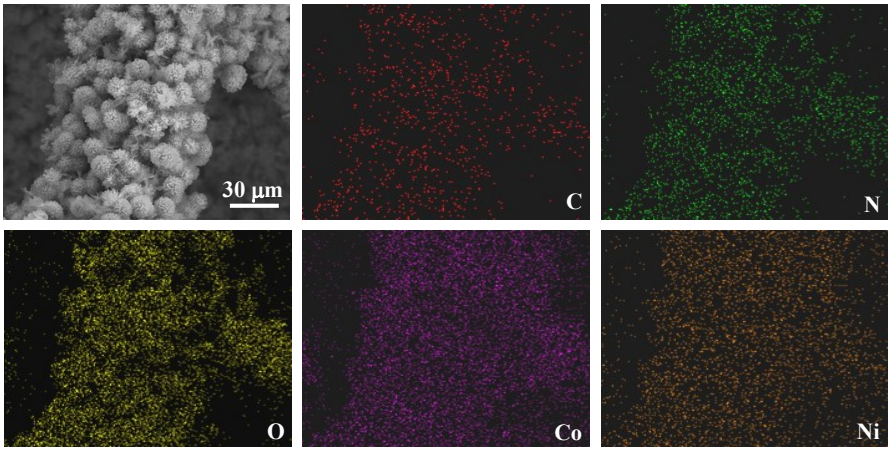

Figure S6. EDS elemental mapping of NCC-NF.

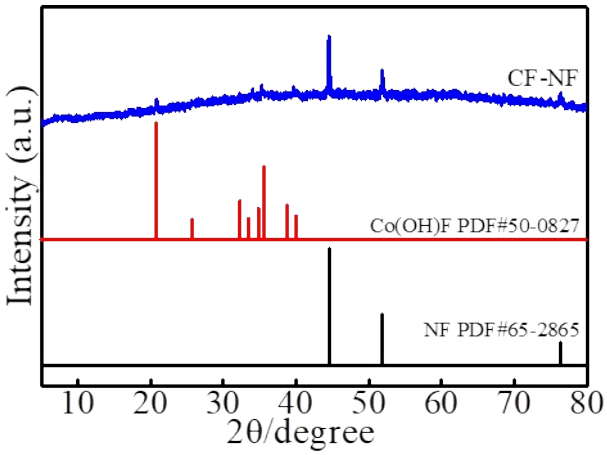

Figure S7. PXRD patterns of CF-NF.

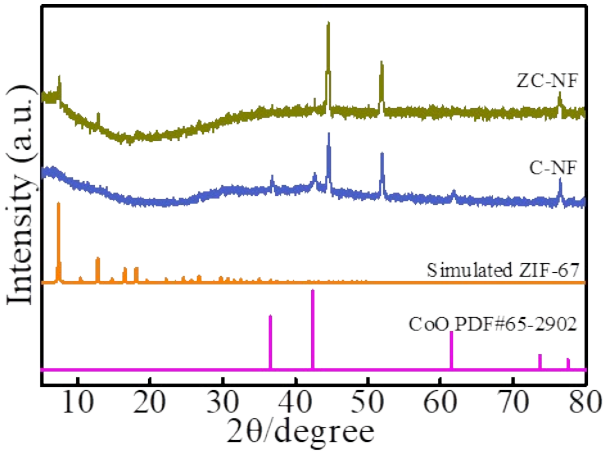

Figure S8. PXRD patterns of C-NF and ZC-NF.

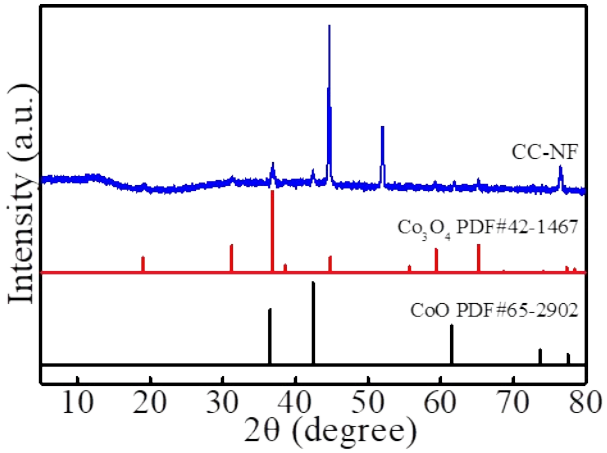

Figure S9. PXRD patterns of CC-NF.

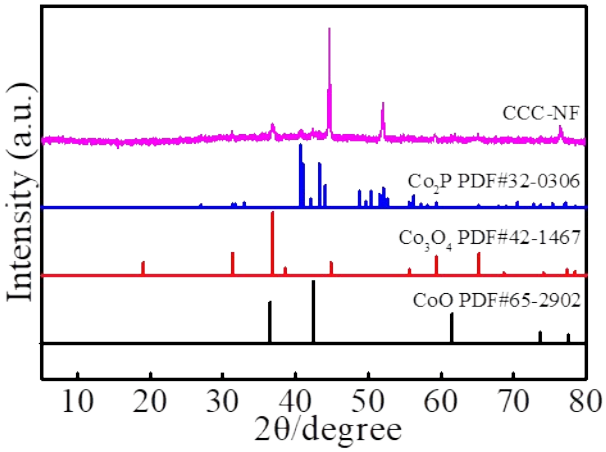

Figure S10. PXRD patterns of CCC-NF.

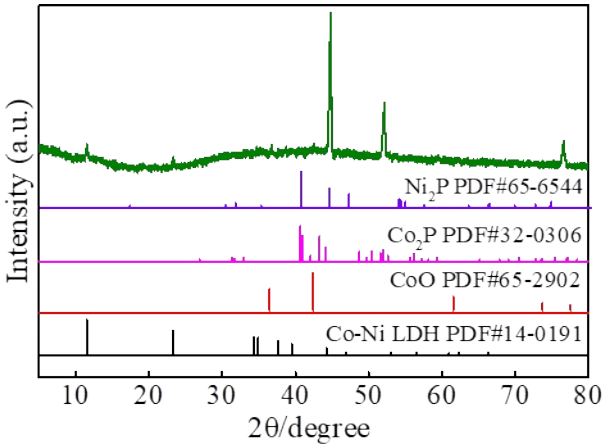

Figure S11. PXRD patterns of P-CNC-NF.

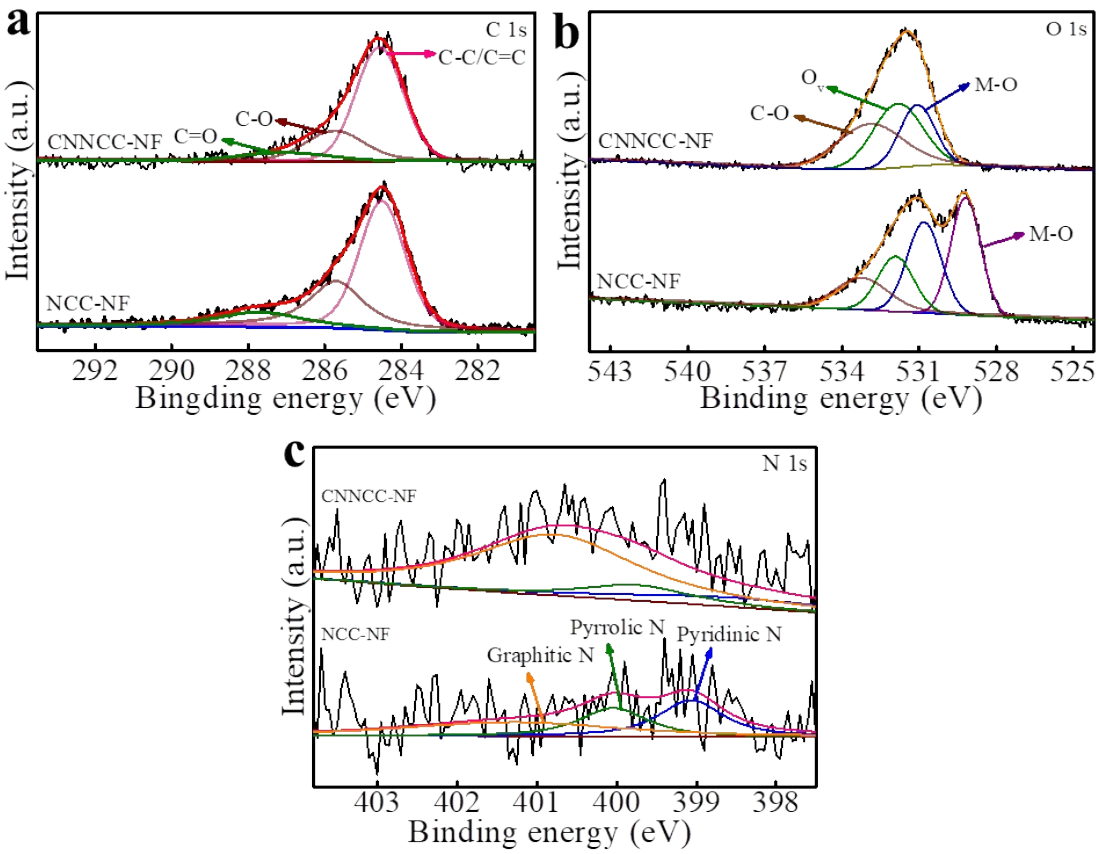

Figure S12. a, b and c) C 1s, O 1s and N 1s high-resolution XPS spectra of NCC-NF and CNNCC-NF.

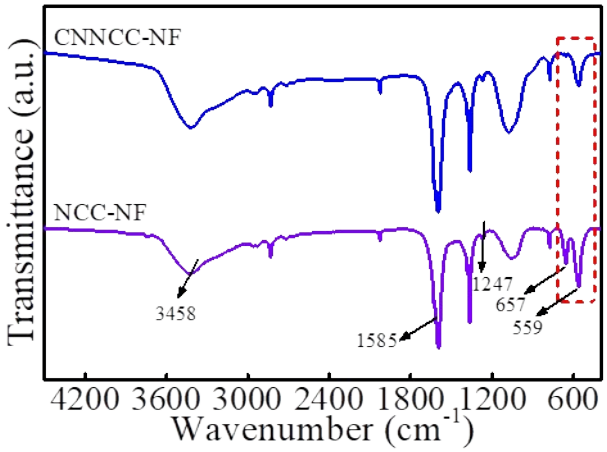

Figure S13. FTIR spectra of NCC-NF and CNNCC-NF.

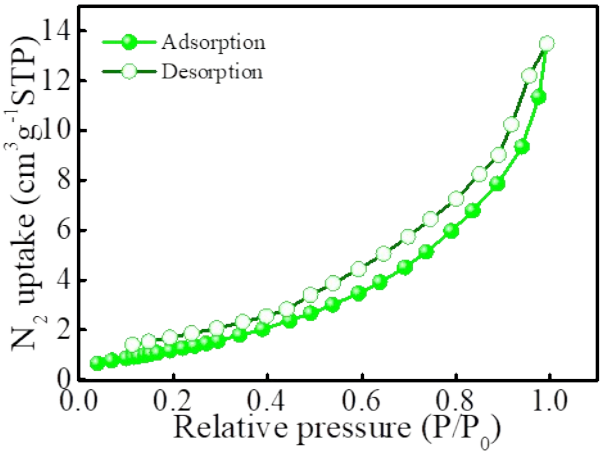

Figure S14. N_2 adsorption-desorption isotherms of C-NF.

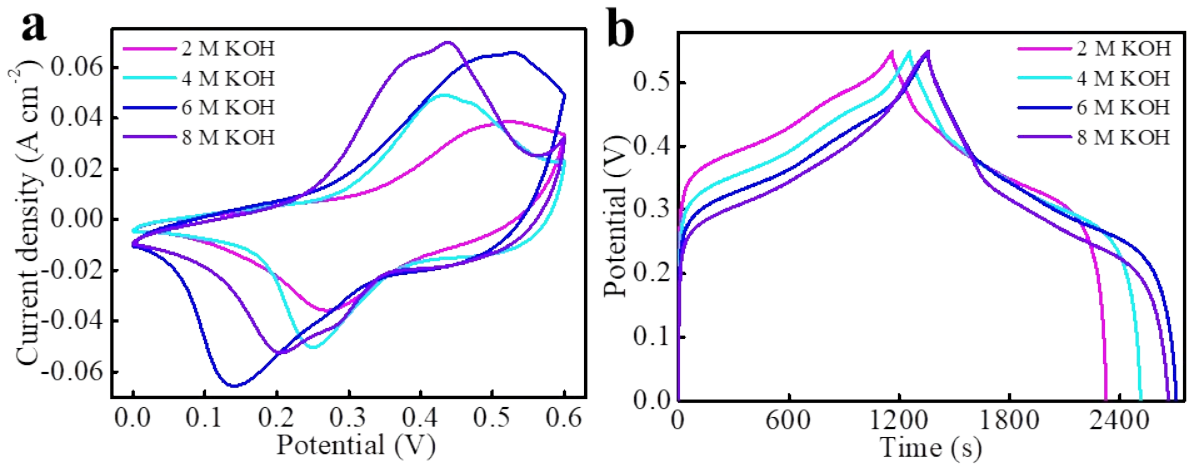

Figure S15. a) CV curves of CNNCC-NF at a scan rate of 2 mV s^{-1}, and b) GCD curves of CNNCC-NF at a current density of 4 mA cm^{-2} in 2, 4, 6, and 8 M KOH.

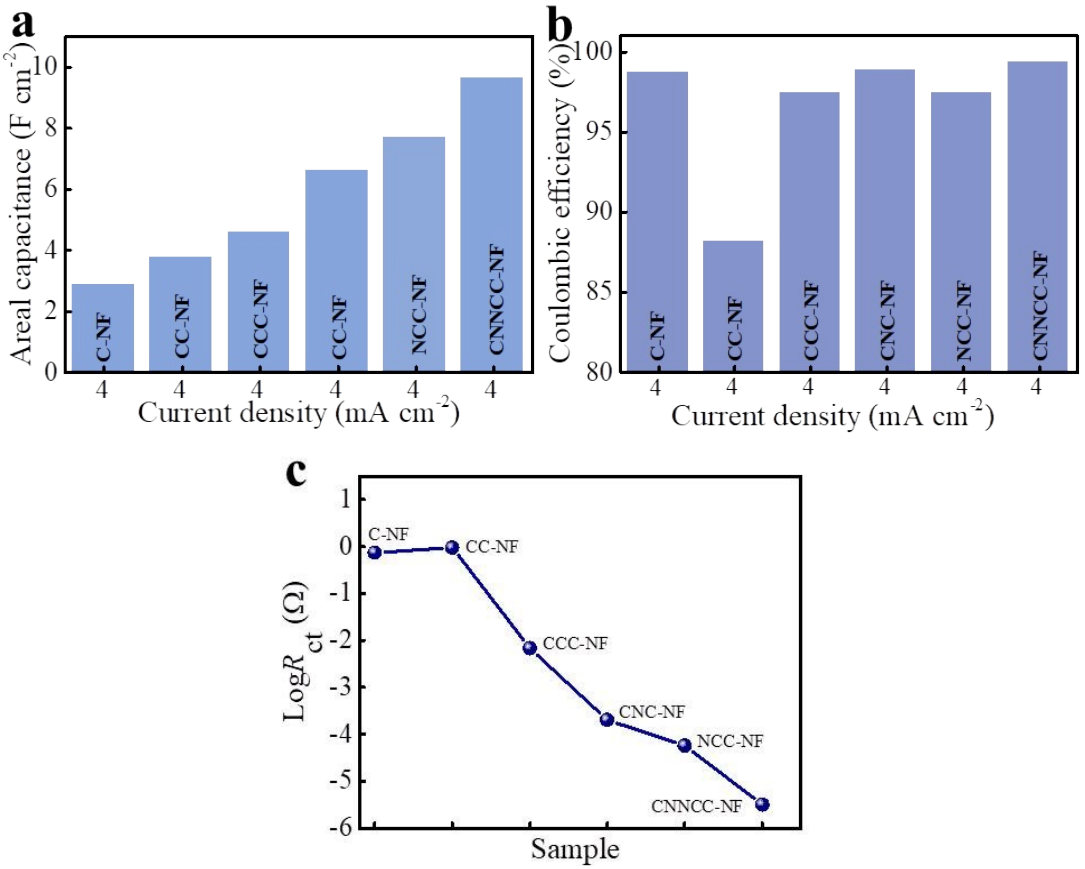

Figure S16. a) Areal capacitance and b) Coulombic efficiency at a current density of 4 mA cm^{-2}, and c) R_{ct} of C-NF, CC-NF, CCC-NF, CNC-NF, NCC-NF and CNNCC-NF.

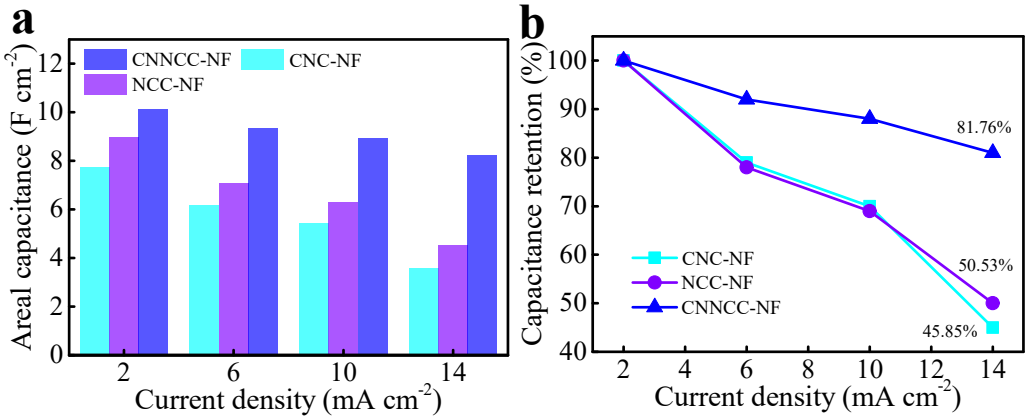

Figure S17. a) Areal capacitance and b) Capacitance retention at different current densities from 2 mA cm^{-2} to 14 mA cm^{-2} of CNC-NF, NCC-NF and CNNCC-NF.

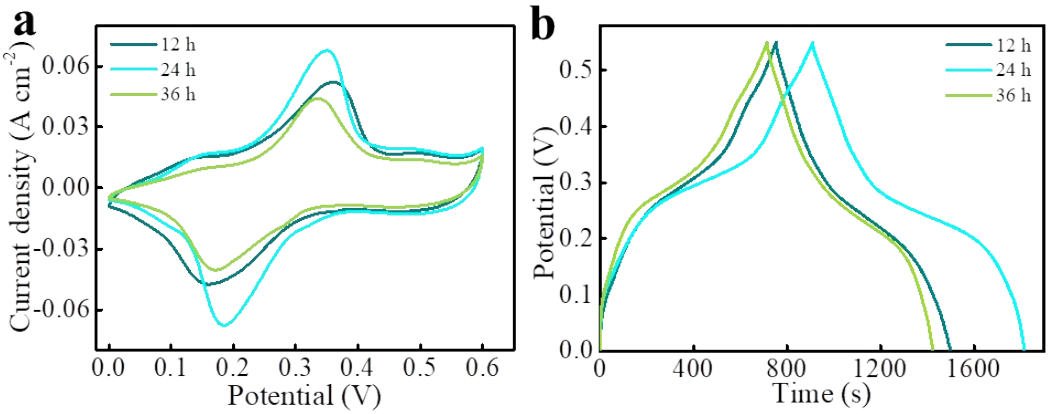

Figure S18. a) CV curves at a scan rate of 4 mV s^{-1}, and b) GCD curves at a current density of 4 mA cm^{-2} of CNC-NF on different etching and ion exchange time from 12 to 36 h.

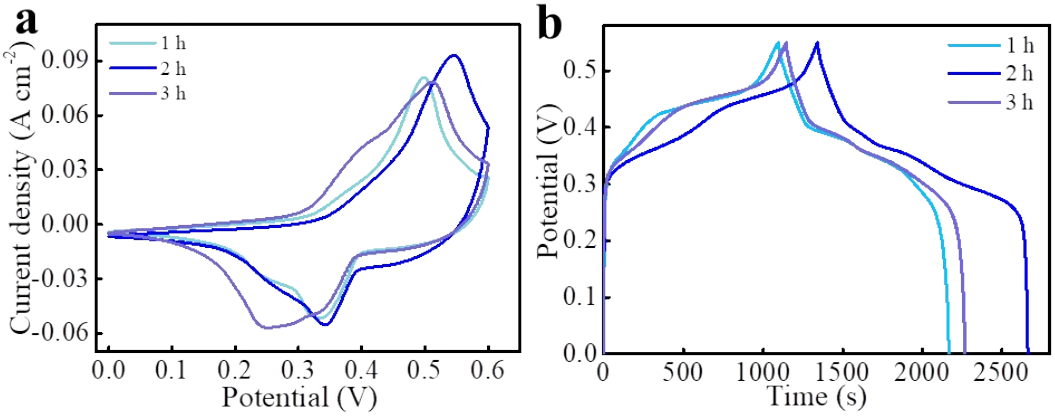

Figure S19. a) CV curves at a scan rate of 4 mV s^{-1}, and b) GCD curves at a current density of 4 mA cm^{-2} of CNNCC-NF on different phosphatization time from 1 to 3 h.

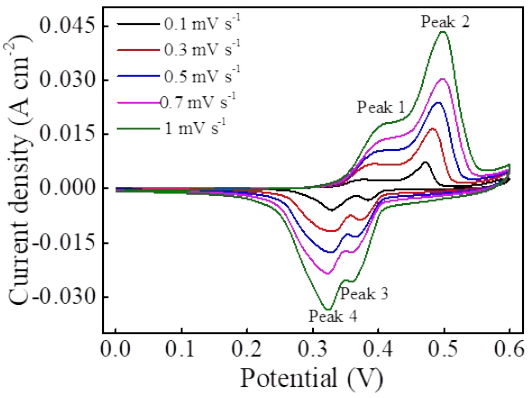

Figure S20. CV curves at different scan rates of CNNCC-NF.

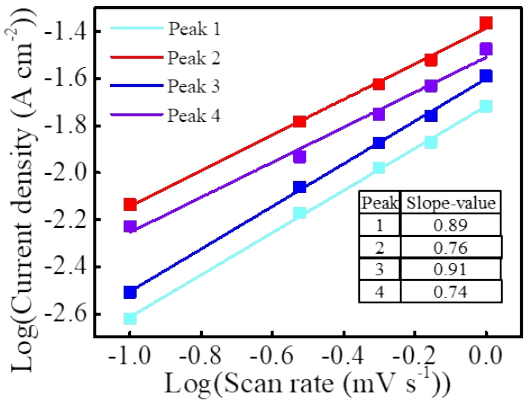

Figure S21. Linear relationship between logarithm of anodic peak current, cathode peak current and logarithm of scan rates.

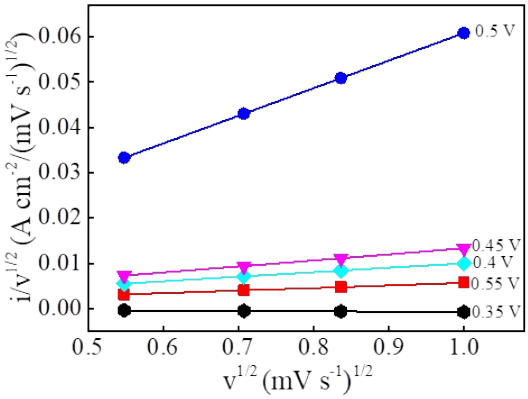

Figure S22. Linear relationship between $i(V)/v^{1/2}$ and $v^{1/2}$ used to calculate the constants of k_1 and k_2 at different potentials of CNNCC-NF.

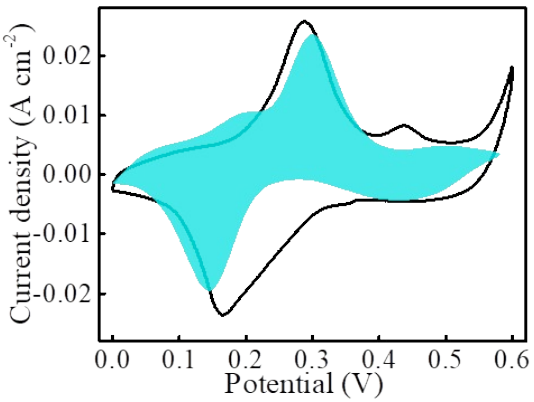

Figure S23. Capacitive charge storage contributions of CNC-NF.

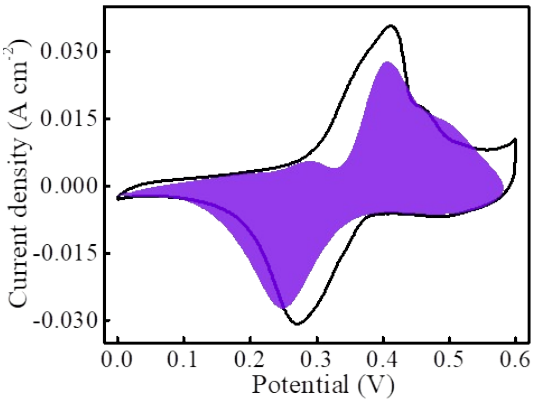

Figure S24. Capacitive charge storage contributions of NCC-NF.

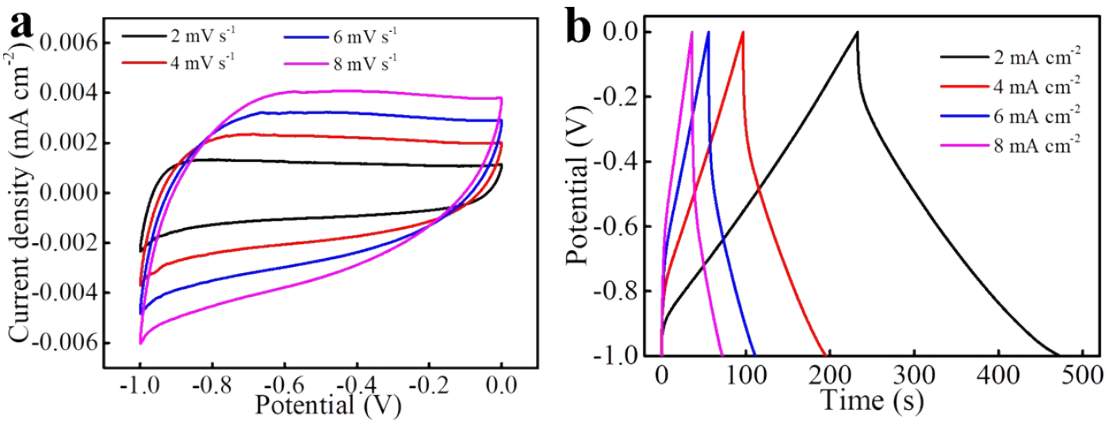

Figure S25. a) CV curves at different scan rates from 2 to 8 mV s^{-1}, and b) GCD curves at different current densities from 2 to 8 mA cm^{-2} of AC-NF.

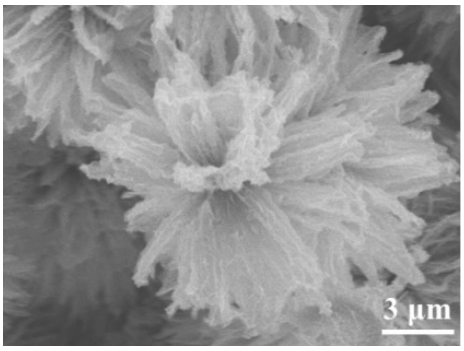

Figure S26. SEM images of CNNCC-NF after 10000 cycles GCD examination.

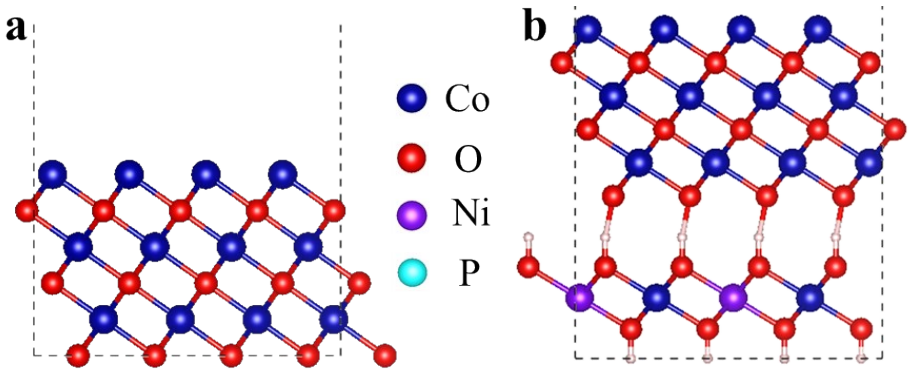

Figure S27. Interfacial compound model of a) C, and b) CNC.

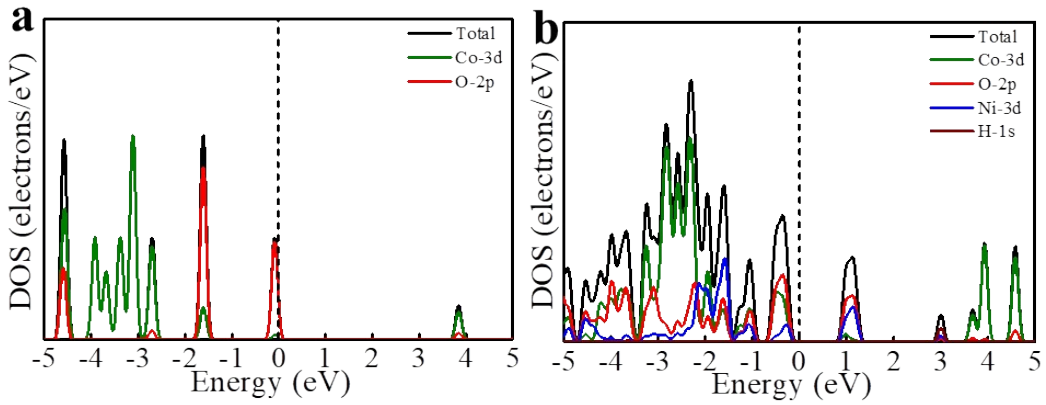

Figure S28. Density of states of a) C, and b) CNC.

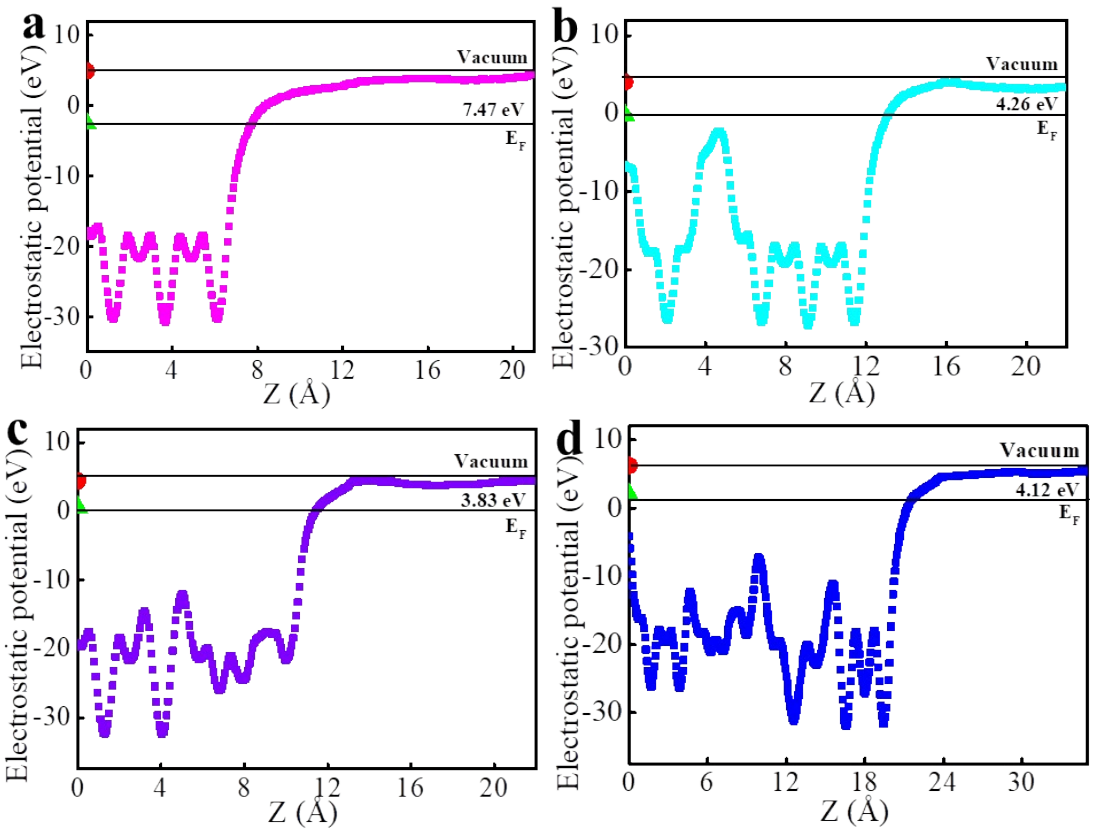

Figure S29. Work function of a) C, b) CNC, c) NCC, and d) CNNCC low-index surfaces.

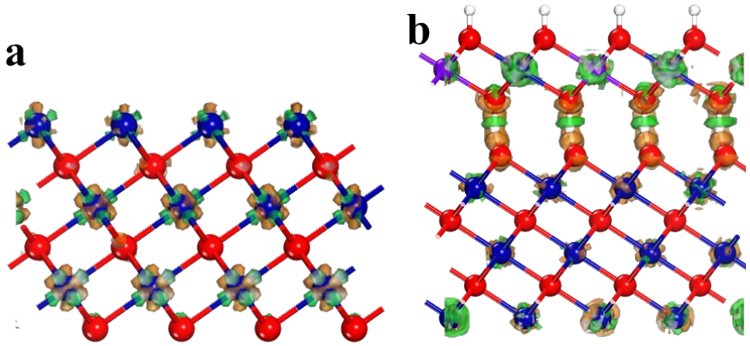

Figure S30. Electron density difference of a) C, and b) CNC.

Table S1. The fitting results of R_s, R_{ct}, C_{dl} and C_{ps} for C-NF, CC-NF, CCC-NF, CNC-NF, NCC-NF and CNNCC-NF electrodes.

Electrodes	R_s	R_{ct}	C_{dl}	C_{ps}
C-NF	0.92	0.75	1.6×10^{-2}	0.17
CC-NF	0.62	0.95	6.4×10^{-2}	0.41
CCC-NF	0.75	6.83×10^{-3}	5.2×10^{-2}	0.20
CNC-NF	0.65	2.03×10^{-4}	1.7×10^{-3}	0.33
NCC-NF	1.39	5.75×10^{-5}	1.6×10^{-3}	0.085
CNNCC-NF	0.71	3.2×10^{-6}	1.3×10^{-3}	0.043

Table S2. Comparison of CNNCC-NF with various Ni/Co based electrodes materials for ASCs.

Type	Morphology	Electrolyte	Current density	Capacitance	Ref.
NiCo-LDH@Au-CuO/Cu	Array	3 M KOH	1.5 mA cm^{-2}	1.97 F cm^{-2}	7
$Co_{1-x}S/CoFe_2O_4$@rGO	Nanoflowers	2 M KOH	1 A g^{-1}	2202 F g^{-1}	8
Ni-Mo-S@Ni-P	Composite	3 M KOH	1 A g^{-1}	1770 F g^{-1}	9
Ni/P/N/C-500	Composites	6 M KOH	1 A g^{-1}	979.8 F g^{-1}	10
Co-Fe-Mn phosphide	Nanoflakes	1 M KOH	2 mA cm^{-2}	4.36 F cm^{-2}	11
CoP	Nanowire	1 M LiCl	1 mA cm^{-2}	571.3 mF cm^{-2}	12
CNNCC-NF	Spiny globe with flat leaves-shaped	6 M KOH	2 mA cm^{-2}	10.11 F cm^{-2}	**This work**
CNNCC-NF	Spiny globe with flat leaves-shaped	6 M KOH	1.05 A g^{-1}	2528.23 F g^{-1}	**This work**

Table S3. The comparative electrochemical performance for ASCs based on the Co/Ni and P-doped electrodes.

Device	Electrolyte	Window (V)	Energy density (Wh kg^{-1})	Power density (W kg^{-1})	Ref.
$Co_{1-x}S/CoFe_2O_4$@rGO//AC	2 M KOH	1.4	61.5	700	Ref. 8
0.1Cu-MOF/$Cu_{2+1}O$//AC	6 M KOH	1.5	25.67	740.4	Ref. 13
Zn-Ni-P-S//AC	3 M KOH	1.6	29.1	275.54	Ref. 9
Co-Fe-Mn phosphide//AC	1 M KOH	1.6	53.2	399.7	Ref. 14
Co_3O_4/NH//AC	2 M KOH	1.5	34.5	753	Ref. 15
P-Co_3O_4@P,N-C//Co@P,N-C	PVA/KOH	1.5	47.6	750	Ref. 11
P-doped MoS_2//MnO_2	PVA/Na_2SO_4	1.7	67.4	850	Ref. 16
CNNCC-NF//AC-NF	6 M KOH	1.6	84.03	364.40	**This work**

References

1 G. Kresse, J. Furthmuller, *Phys. Rev. B,* 1996, **54**, 11169-11186.

2 G. Kresse, J. Furthmuller, *Comput. Mater. Sci.,* 1996, **6**, 15-50.

3 J. P. Perdew, K. Burke, M. Ernzerhof, *Phys. Rev. Lett.,* 1997, **78**, 1396-1396.

4 G. Kresse, D. Joubert, *Phys. Rev. B,* 1999, **59**, 1758-1775.

5 P. E. Blochl, *Phys. Rev. B,* 1994, **50**, 17953-17979.

6 S. N. Steinmann, C. Corminboeuf, *J. Chem. Theory Comput.,* 2010, **6**, 1990-2001.

7 Y. Guo, X. Hong, Y. Wang, Q. Li, J. Meng, R. Dai, X. Liu, L. He, L. Mai, *Adv. Funct. Mater.,* 2019, **29**, 1809004.

8 C. Ren, X. Jia, W. Zhang, D. Hou, Z. Xia, D. Huang, J. Hu, S. Chen, S. Gao, *Adv. Funct. Mater.,* 2020, **30**, 2004519.

9 X. Lei, S. Ge, T.-Y. Yang, Y. Lu, Y.-L. Chueh, B. Xiang, *J. Power Sources,* 2020, **477**, 229022.

10 F. Yu, X. Xiong, L.-Y. Zhou, J.-L. Li, J.-Y. Liang, S.-Q. Hu, W.-T. Lu, B. Li, H.-C. Zhou, *J. Mater. Chem. A,* 2019, **7**, 2875-2883.

11 R. Niu, G. Wang, Y. Ding, S. Tang, X. Hu, J. Zhu, *J. Mater. Chem. A,* 2019, **7**, 4431-4437.

12 N. Zhang, J. Xu, B. Wei, J. Li, I. Amorim, R. Thomas, S. M. Thalluri, Z. Wang, W. Zhou, S. Xie, L. Liu, *ACS Appl. Energy Mater.,* 2020, **3**, 4580-4588.

13 X. Cao, L. Cui, B. Liu, Y. Liu, D. Jia, W. Yang, J. M. Razal, J. Liu, *J. Mater. Chem. A,* 2019, **7**, 3815-3827.

14 S. Liu, Y. Yin, Y. Shen, K. S. Hui, Y. T. Chun, J. M. Kim, K. N. Hui, L. Zhang, S. C. Jun, *Small,* 2020, **16**, 1906458.

15 T. Liu, L. Zhang, W. You, J. Yu, *Small,* 2018, **14**, 1702407.

16 S. Liu, Y. Yin, M. Wu, K. S. Hui, K. N. Hui, C.-Y. Ouyang, S. C. Jun, *Small,* 2019, **15**, 1803984.